Anisotropic Ion Migration and Electronic Conduction in van der Waals Ferroelectric $CuInP_2S_6$

Dawei Zhang,[1,#] Zheng-Dong Luo,[2,#,*] Yin Yao,[3] Peggy Schoenherr,[1,4] Chuhan Sha,[1] Ying Pan,[1] Pankaj Sharma,[1,4] Marin Alexe,[2] Jan Seidel[1,4,*]

[1] School of Materials Science and Engineering, UNSW Sydney, Sydney NSW 2052, Australia

[2] Department of Physics, The University of Warwick, Coventry CV4 7AL, United Kingdom

[3] Electron Microscopy Unit (EMU), Mark Wainwright Analytical Centre, UNSW Sydney, Sydney, NSW 2052, Australia.

[4] ARC Centre of Excellence in Future Low-Energy Electronics Technologies (FLEET), UNSW Sydney, Sydney 2052, Australia

ABSTRACT: Van der Waals (vdW) thio- and seleno-phosphates have recently gained considerable attention for the use as 'active' dielectrics in two-dimensional/quasi-two-dimensional electronic devices. Bulk ionic conductivity in these materials has been identified as a key factor for the control of their electronic properties. However, direct evidence of specific ion species' migration at the nanoscale, particularly under electric fields, and its impact on material properties has been elusive. Here, we report on direct evidence of a phase-selective anisotropic Cu ion hopping mechanism in copper indium thiophosphate ($CuInP_2S_6$) through detailed scanning probe microscopy measurements. A two-step Cu-hopping path including a first intralayer hopping (in-plane) and second interlayer hopping (out-of-plane) crossing the vdW gap is unveiled. Evidence of electrically controlled Cu ion migration is further verified by nanoscale energy-dispersive X-ray spectroscopy (EDS) mapping. These findings offer new insight into anisotropic ionic manipulation in layered vdW ferroelectric/dielectric materials for emergent vdW electronic device design.

KEYWORDS: *copper indium thiophosphate, van der Waals ferroelectrics, ion migration, ionic conduction*

The rapid growth of two-dimensional (2D) semiconductor devices has spurred burgeoning interest in searching for functional dielectrics that can be integrated with 2D materials like graphene and transition-metal dichalcogenides (TMDs) for device performance enhancement and engineering-rich functionalities.[1-20] Copper indium thiophosphate $CuInP_2S_6$ (CIPS), one of the van der Waals (vdW) ferroelectrics from the transitional metal thio/seleno-phosphates (TPS) family, allows such interface integration to build full-vdW heterostructure based functional logic and memory devices, such as negative capacitance field-effect transistors (NC-FETs),[21] ferroelectric tunnel junctions (FTJs),[22, 23] and ferroelectric field-effect transistors (Fe-FETs).[5, 10, 11] In these devices, the local response of CIPS to the electric field is thus of paramount importance to determine the device performance. Additionally, CIPS has been known to possess considerable electric-field controllable macroscopic ionic conductivity,[1, 24-27] whose coupling with ferroelectricity could lead to novel electrochemical phenomena such as ferroionic states that represent the nonlinear electrostatic coupling between ions and polarization.[28, 29] However, its nanoscale ionic and electronic properties, such as the local conductivity as well as its coupling with ferroelectricity, remain largely unexplored. Gaining a better understanding and control over the nanoscale ionic conductivity in these materials could shed light on new possibilities for CIPS-based electronic devices and may pave the way to the design of more functional vdW heterostructures.[30-33]

With a Curie temperature T_C of 310 K,[6, 34] CIPS single crystals undergo a first-order order-disorder phase transition (from $C_{2/c}$ to C_c) due to the antiparallel displacement of Cu^+ and In^{3+} from their respective octahedral cages.[35] The crystal structure of $CuInP_2S_6$ can be described as a sulfur framework in which metal cations (Cu and In) and P-P pairs fill the octahedral voids, as shown in Figure 1a. It is noteworthy that when Cu is deficient, the system undergoes a chemical phase separation into a paraelectric $In_{4/3}P_2S_6$ phase and a ferroelectric $CuInP_2S_6$ phase.[6] The crystallographic positions taken by the Cu atom are closely related to the emergence of ferroelectricity and its ionic conductivity. In the paraelectric phase ($T>T_C$), the Cu^{1+} atom can occupy and vertically move among three partially filled crystallographic sites (Figure 1b): (1) Cu1-quasitrigonal, at off-centered positions; (2) Cu2-octahedral, close to octahedron centers; (3) Cu3-almost tetrahedral, penetrating into the interlayer (vdW gap)

space.[35] Furthermore, Cu1 has two possible positions, displaced upward and downward from the middle of the layer (octahedron centers). In the ferroelectric phase ($T<T_C$), Cu1 ions are preferentially displaced in the upward state and thus generate an off-centered Cu displacement coupled with a compensatory antiparallel shift of the In^{3+} sublattice, resulting in an out-of-plane polarization. The hopping of Cu1 ions between the upward/downward positions (in a double minimum potential) is believed to be the reason for the phase transition.[26, 27, 35] It has been argued that the Cu ion hopping, which is enabled by the coupling between Cu1 vibrations and P_2S_6 deformation modes, leads to the onset of ionic conductivity, which shows a thermally activated behavior.[27, 36]

Experimentally, the DC conductivity of CIPS has been determined via dielectric measurements and found to follow Arrhenius behavior with an activation energy for ionic conductivity E_A of: (1) E_A=0.92 eV/0.61 eV (out-of-plane (OOP)/in-plane (IP) when $T>T_C$); (2) E_A=1.16 eV/0.55 eV (OOP/IP when $T<T_C$).[25] The large difference between the E_A in the OOP and IP directions clearly indicates that a higher energy is required for Cu^{1+} ions to hop between interlayer sites (across the layers) than between the intralayer sites (within the layers). Recently, Brehm et al. have both theoretically and experimentally verified CIPS as a 'quadruple-well' ferroelectric providing multiple potential minima for Cu ion displacements with shallow energy barriers.[4] Particularly, the second potential minimum for the Cu atom, which is enabled by the location within the vdW gap, has brought about a second, high polarization phase. This discovery showcases the mobile nature of Cu atoms, which can hop between intralayer and interlayer sites in the OOP direction.

Despite all those theoretical and experimental reports, no direct evidence has been brought forward yet for nanoscale ionic conductivity in CIPS and how it influences local material properties. Instead, bulk CIPS was found to be quite insulating at room temperature. One reason might be the finite ion migration at room temperature, although the onset temperature of ionic conductivity is around 250 K.[1] However, it is well known that charged ions can become mobile under high electric fields.[37] Moreover, very recently Neumayer et al.[38] have reported that both an electric field and an excess of Cu ions/Cu vacancies can effectively lower the energy barrier and thus facilitate the interlayer Cu hopping that crosses

the vdW gap at room temperature, which ultimately corroborates the room-temperature ionic conduction due to long-range migration of Cu ions. In this study, we thus investigate CIPS as a model system of the TPS family to gain insight into the nanoscale ionic conductivity. We report on phase-selective electrical conduction on the nanoscale using conductive atomic force microscopy (c-AFM). Using nanoscale energy-dispersive X-ray spectroscopy (EDS), for the first time, direct evidence of electrically controlled Cu ion migration and accumulation at nanoscale biased areas is shown. Detailed in-situ current measurements under alternating bias further reveal an anisotropic Cu ion hopping mechanism as the origin of the observed ionic conduction behavior.

The Cu-deficient $CuInP_2S_6$ single crystals studied here have an average chemical composition of $Cu_{0.2}In_{1.26}P_2S_6$ (Cu/In ratio around 0.16 see EDS results in Table S1) with a Curie temperature of ~330 K.[6] The Cu-deficient CIPS sample exhibits a local chemical phase separation presenting both Cu-free paraelectric $In_{4/3}P_2S_6$ (IPS) phase and ferroelectric $CuInP_2S_6$ (CIPS) phase. By virtue of the phase coexistence, the Cu ion mobility and migration can be directly assessed in the CIPS phase, whereas the Cu-free IPS phase provides an ideal reference for ionic conductivity measurements. CIPS flakes ranging from 30 nm to 400 nm were directly exfoliated from the CIPS single crystal through a Scotch tape based exfoliation method and taped onto Au (15 nm)/Poly(methyl methacrylate) (PMMA) (50 nm) coated polyethylene naphthalate (PEN) substrates, see Figure 1c for the detailed sample configuration. Figure 1d shows the smooth topography of a representative CIPS flake indicating that the exfoliated sample preserves a high-quality single crystalline structure after the fabrication process. The coexistence of CIPS and IPS phases in the Cu-deficient CIPS flake is clearly demonstrated by corresponding piezoresponse force microscopy (PFM) images, see Figures 1e-h. The thickness of the studied flake is around 130 nm. A clear 180° phase difference is observed between the upward- and downward- polarized ferroelectric domains within the CIPS phase (Figure 1e and Figure 1g), which confirms the ferroelectricity of the CIPS phase. The PFM measurements can further identify the phase separation in the sample by closely looking into the piezoresponse of different regions within the flake.[39] As shown in Figure 1f and Figure 1h, the CIPS ferroelectric phase having a branch-like structure

exhibits a high piezoresponse and the IPS paraelectric phase shows a negligible piezoresponse.

We further employed conductive atomic force microscopy (c-AFM) to probe the nanoscale electrical properties of the CIPS flake. Figure 2a shows the piezoresponse of a region with coexisting CIPS and IPS phases, and its corresponding c-AFM image scanned at -3 V is revealed in Figure 2b. Surprisingly, the whole CIPS phase is quite conducting compared to the insulating IPS phase surrounding it, see Figures 2b, which is associated with the existence of Cu ions in the CIPS phase. We did not find an exact one-to-one correlation between the nanoscale conductance variations in the CIPS phase and the ferroelectric domains and walls as has been reported for many of the standard oxide ferroelectrics, and/or multiferroics.[40, 41] More interestingly, the conductivity of the CIPS phase shows a widely observed activation behavior, i.e., the conductivity becomes enhanced with decreasing scanning speeds or increasing measurement cycles, which is reminiscent of other well-known ionic conductors such as $KTiOPO_4$.[42] The scanning-speed related conductivity change of CIPS is shown in Figures 2c-d where the current line profiles are extracted from the same area scanned by different speeds (2 μm/s and 0.5 μm/s), as denoted by the white dashed box in Figure 2b. Approximately, a ~60-fold enhancement of the current amplitude can be obtained on the CIPS phase when reducing the tip scanning speed from 2 μm/s to 0.5 μm/s (also see Figure S1), suggesting an electrically controlled electrochemical ion migration behavior. In order to gain a better understanding of such an ion migration mediated conductivity change, I-V curves measured on different phases of the CIPS flake were obtained by bias ramping of 0 V→-8 V→+8 V at a ramp speed of 2 V/s. The CIPS and IPS phases show distinctive transport behavior as can be seen in Figure 2e. In the inset of Figure 2e, three different I-V responses of the CIPS phase, obtained with different voltage ramp speeds (0.5 V/s, 1 V/s, and 2 V/s) at three adjacent points, further reveal the behavior of electrically controlled conductivity. Such conductivity evolvement as manifested by higher current at a slower ramp speed (conductivity activation) can be attributed to time-dependent Cu ion movement under electric fields, as a lower scan rate allows migrating ions to experience the electric bias from the AFM tip for an effectively longer time, therefore

generating a higher carrier concentration and current.[42] In addition, time-dependent conductivity measurements on both CIPS and IPS phases were performed. The AFM tip with a DC bias of –4 V was kept at fixed positions on respective CIPS and IPS phases while the current was recorded for 300 s, as shown in Figure 2f. The current of the IPS phase is almost zero and remains stable during the measurement, while in stark contrast, the current of the CIPS phase increases steadily throughout the recording time. The increasing current with time further demonstrates the dynamics of ion migration/accumulation within the CIPS phase under the biased tip. Overall, the electrically tunable nanoscale ionic conductivity in the CIPS phase has been clearly observed and corroborated via the electrical measurements.

Reversible/irreversible topographic changes and formed surface particles caused by the ion accumulation are known to be a concomitant phenomenon during ion migration in ionic conductors, especially in CIPS.[38, 43-45] Consequently, how long-range Cu ion migration will collectively influence the material's macroscopic structure needs to be examined. Therefore firstly, topography images of the CIPS flake were acquired after the application of a long-time DC electric field at tip-contact area. The SPM tip with different biases was fixed at four points nearby in the CIPS phase for 300 s, and the simultaneous current values were recorded together with the subsequent topography changes, as shown in Figure S2. Surface depressions were created on the sample surface after this sustained voltage application. The diameters and depths of the circular surface depressions are proportional to the holding time as well as the voltage amplitude. The surface depression after the bias poling is presumably related to the local structural changes regarding the CIPS/IPS phase redistribution, which results from the electrically driven long-range scale Cu ions migration away from their equilibrium positions considering the electric field itself as a large perturbation.[6, 38] Figure 3 shows the morphological changes with the dependence of tip voltages under air and N_2 atmosphere. Consistent changes are seen in both atmospheres, which rules out the possible interference from the formation of metal oxides. The accumulative effect of the Cu ion migration is shown as progressive surface depression with increasing tip biases. Since the onset of ionic conductivity has been reported to be around 250 K, faster and more pronounced changes are expected at higher temperatures because of the thermally activated Cu ion movement. Our

observation of topographical changes further corroborates the long-range movement of the Cu ions at room temperature. In Figures S4a-b, c-AFM images conducted at +6 V and -6 V show a non-conductive and a highly conductive CIPS phase, respectively. Furthermore, in Figure S5, a series of I-V curves with different sweep speeds (0.5 V/s, 1 V/s, and 2 V/s) each consisting of three consecutive cycles from 0 V→-8 V→+8 V→0 V were performed on the same spot of the CIPS phase. They all show a consistent trend of decreasing negative maximum current values at each cycle because of a time-dependent Cu ion migration under different polarities of biases. More discussions can be seen in the Supporting Information Figure S5 and Figure S6.

The chemical composition of the bias-induced depression structure is of particular interest as it may provide direct evidence for the long-range Cu ion migration. Therefore, scanning electron microscope (SEM) and energy dispersive spectroscopy (EDS) were carried out to probe the created depression structure on the CIPS sample surface. Prior to the SEM investigation, the sample was poled by a conductive scanning probe microscopy (SPM) tip to accumulate Cu ions in the CIPS phase. A DC voltage (-6 V here) was applied to the tip and it was sufficient to generate and maintain an average current of around -100 pA on the CIPS phase. The same area was scanned with bias 30 times consecutively to attract enough Cu ions for better EDS signals. The PFM amplitude image (acquired by 0.5 V AC voltage) in Figure 4a shows the as-grown state of the sample area before the application of the DC voltage, in which the CIPS phase shows clear piezoresponse signal. After the poling, the morphology (see Figure 4b) shows a subsided structure of around -2.5 nm corresponding to the biased CIPS phase, which is attributed to the induced Cu ion migration. The Cu-rich signal from the EDS mapping evidently manifests the accumulation of Cu ions at the biased CIPS region, as shown in Figure 4c. The Cu EDS mapping correlates very well with the CIPS phase in Figure 4a. In contrast, chemically homogeneous distributions for other elements were observed without any evidence of local enrichment as shown in Figure S7. Moreover, no metal oxides were observed based on the O mapping in Figure S7h. To note, a few cracks were formed on the sample surface during the EDS mapping as the CIPS is quite sensitive to the electron beam, as shown in Figure S7a. Moreover, EDS mappings were also performed on a sample with

a shorter poling time (10 times) under the same experimental conditions. The sample shows a much weaker concentration of Cu that, however, still visibly corresponds to the CIPS phase (shown in Figure S8). Also, the EDS mapping on a reference area that was not poled was investigated. The size for the reference area (3.8 μm×2.8 μm) is large enough to include CIPS phases. The EDS results (Figure S9) show a quite homogeneous distribution for all the elements, indicating no apparent Cu ion accumulation at the unpoled CIPS phase. Thus, all these EDS experiments unequivocally prove a time dependent electrically driven Cu ion migration in the studied sample.

In the vertical direction, the Cu ion hopping between the intralayer and interlayer sites and even across the vdW gap is known to be the reason for the macroscopic ionic conductivity.[38] As indicated by the aforementioned activation energy results for the Cu ion motion and conduction, the Cu ion movement could also occur at the horizontal direction. To further explore the Cu ion migration mechanism and its effect on electrical properties of the CIPS phase, local current versus time measurements were performed. Three separate current measurements with repetitive bias-on (60-second, -8 V) and bias-off cycles with varied durations (30-second for Figure 4d, 1-second for Figure 4e, and 60-sescond for Figure 4f) were recorded as a function of time at the same location on the CIPS phase. Given the aforementioned ionic conductivity activation phenomenon with the application of DC bias, a sufficiently long wait time (30 min) was introduced between every scan to allow for a full relaxation of the activated ions. For the first 60-second bias-on period shown in Figures 4d-f, the maximum current values are very comparable with each other being -11 pA, -14 pA and -17 pA, respectively. This phenomenon of current relaxation with time is another strong evidence for ionic dynamics.[46-48] Figure 4d shows the activated conductivity between each bias-off and bias-on cycle: the current falls to zero when the bias is removed, and it quickly increases to a high value once the bias is on. Figure 4g shows a zoom-in image of Figure 4d with the time window between 230 s to 330 s. During the bias-on cycle, the current quickly boosts to around -12 pA showing a large slope within the first 5 seconds, denoted as ‘stage I’, and then undergoes a slower increasing with a decreased slope, denoted as ‘stage II’. This two-stage characteristic is likely to be associated with two paths for the Cu migration.

Previous research shows that the activation energy values for both Cu ion motion (E_a) and Cu ionic conductivity (E_A) are higher in the OOP direction than those in the IP direction with E_a=0.85 eV/0.23 eV (OOP/IP)[6] and E_A=1.16 eV/0.55 eV (OOP/IP $T<T_C$)[25]. The relationship between the Cu ion motion/hopping activation energy and ion conductivity energy can be expressed as $E_A=E_a+E_C$ where E_C is the activation energy for the creation of mobile carriers.[24] Apparently, driving the Cu ion to hop between and across the layers as well as initiating the ionic conductivity (in the OOP direction) requires more energy than within the layer (in the IP direction). Hence, for stage I, the current increase is dominated by the IP Cu ion migration. The large current boost seen here is attributed to the quick IP reassembly of Cu ions previously attracted and aggregated around the tip-sample contact during the last bias-on cycle. The IP Cu ion migration takes place first because of the smaller required energy. For stage II, the current increase is dominated by the Cu ions hopping along the OOP direction. The slope is thus smaller because it takes a longer time for the Cu ions to migrate across layers through the sample to the biased area. In Figure 4e, only stage II is shown in the curve because the 1-second bias-off cycle is so short that the reassembling process is absent, leading to an instantaneous conduction. It is found that the slopes for stage II in Figures 4d-f are almost identical, indicating the exact same speed for Cu ion migration along the polar axis. To conclude, two hopping/migration paths for Cu ions have been established by the local current measurements: the IP intralayer hopping and the OOP interlayer hopping that involves vdW gap crossings. The schematic illustration of the proposed Cu ion migration model is shown in in Figure 4h. Migration paths in both OOP and IP directions are shown by the arrows. The Cu ions are still migrating atop the CIPS region under the DC bias despite the local surface depression. It should be noted that the time-dependent conduction behavior of the CIPS unambiguously indicates the dominant ionic conduction caused by the Cu ion migration under the large electric field, though the bias-separated Cu ions and Cu vacancies in the CIPS could locally induce *p-n* diode like electronic conduction. More details have been discussed in Figure S10 and Figure S11.

Our observation shows a high degree of consistency with previously reported theory and results. In the OOP direction, the recently discovered quadruple potential well in CIPS

provides a solid theoretical foundation for the long-range Cu ion migration as the Cu can move into the vdW gap and form interlayer bonds with S atoms from adjacent layers.[4] Besides, the presence of the electric field and the excess of Cu vacancies can lower the activation energy barrier and thus facilitate the unidirectional interlayer Cu hopping that involves the vdW gap crossing.[38] In our Cu-deficient CIPS, a higher concentration of Cu vacancies is expected compared to the stoichiometric CIPS, which is consistent with the observed clear ionic conductivity. In the IP direction, there are six crystallographically equivalent sites in the S6 octahedron for the Cu ion hopping. The hopping between two adjacent Cu ion sites is facile considering the relatively low energy barrier.[9] Therefore, by the application of a large spatial DC electric field under the tip, long-range Cu ion migration takes place and leads to ionic conductivity in the CIPS.

In summary, we report on nanoscale ionic conduction in Cu-deficient CIPS as confirmed by the c-AFM results, which is found to be correlated with the hopping motion of Cu ions driven by the applied electric field. Concomitant topographical changes as surface depressions have been observed due to long-range Cu ion migration. Subsequent nanoscale EDS mappings of the morphological changes substantiate the accumulation of Cu ions by showing a clear Cu-rich contrast at the exact area of the CIPS phase after the applied negative DC bias. Afterwards, through local current measurements, a two-step path for Cu ion migration has been unveiled, indicating first an IP intralayer and second an OOP interlayer hopping motion. The coexistence and interplay of ferroelectricity and ionic conductivity in phase-separated CIPS and nanoscale manipulation of their electrical properties may stimulate new ideas and concepts for the tuning and coupling of ferroelectric and electronic properties in two-dimensional vdW ferroelectric devices.

ASSOCIATED CONTENT

Supporting Information

The Supporting Information is available free of charge at https://pubs.acs.org/doi/

Experimental sections; $CuInP_2S_6$ composition determined by EDS; scanning-speed dependent current signal; surface depression as a function of applied tip bias and holding time; PFM analysis of the depression area; the migration behavior of Cu ion under different polarities of biases; EDS results on regions with different poling time; discussion of ionic and electronic conduction in the CIPS; Cu ion relaxation process; EDS probing depth and resolution.

AUTHOR INFORMATION

Corresponding Authors

Zheng-Dong Luo - *Department of Physics, The University of Warwick, Coventry CV4 7AL, United Kingdom;* Email: luozhengdong7@gmail.com

Jan Seidel - *School of Materials Science and Engineering, UNSW Sydney, Sydney NSW 2052, Australia; ARC Centre of Excellence in Future Low-Energy Electronics Technologies (FLEET), UNSW Sydney, Sydney 2052, Australia;*
Email: jan.seidel@unsw.edu.au

Author Contributions

[#]D.Z. and Z.-D.L. contributed equally to this work.

Notes

The authors declare no competing financial interest.

ACKNOWLEDGMENTS

We thank the helpful discussion with M.Z.. We acknowledge support by the Australian Research Council through Discovery Grants and the ARC Center of Excellence in Future Low Energy Electronics Technologies (FLEET). D.Z. acknowledges an Australian Government Research Training Program Scholarship. Y.P. acknowledges the China Scholarship Council (CSC) for financial support [no. 201604910910]. M.A. and Z.D.L. acknowledge EPSRC

support via grant no. EP/T027207/1. The authors acknowledge the facilities and the scientific and technical assistance of Microscopy Australia at the Electron Microscope Unit (EMU) within the Mark Wainwright Analytical Centre (MWAC) at UNSW Sydney.

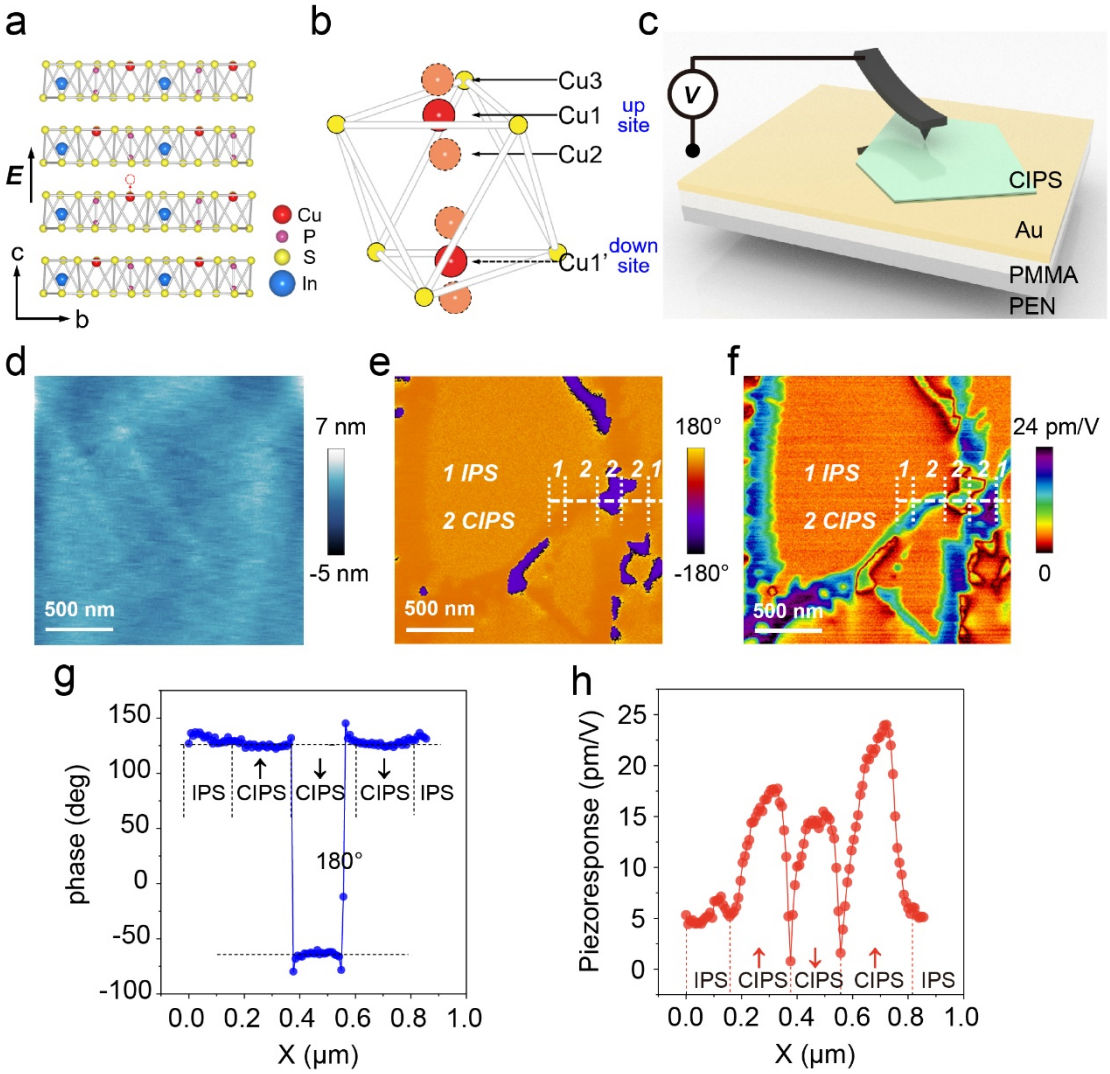

Figure 1. PFM analysis of the CIPS flake and schematic of the sample. (a) The in-plane view of the $CuInP_2S_6$ crystal structure is also shown with vdW gap between the layers. Under the electric field, besides the intralayer hopping, the mobile Cu ion can move into and cross the vdW gap achieving the interlayer hopping. (b) The positions of three copper positions are labelled as Cu1, Cu2 and Cu3. The upward and downward sites for Cu1 are also denoted. (c) Schematic of the sample. The cleaved CIPS flake is transferred onto a PMMA/PEN substrate sputtered with a gold bottom electrode. (d) Topography of the CIPS. (e) Out-of-plane PFM phase and (f) amplitude signals (at resonance frequency) of the sample, respectively. Horizontal dashed lines combined with vertical dashed lines traverse and divide the chemically separated CIPS and IPS phases, marked as 1 and 2. PFM phase (g) and amplitude (h) line profile signals as indicated in (e) and (f).

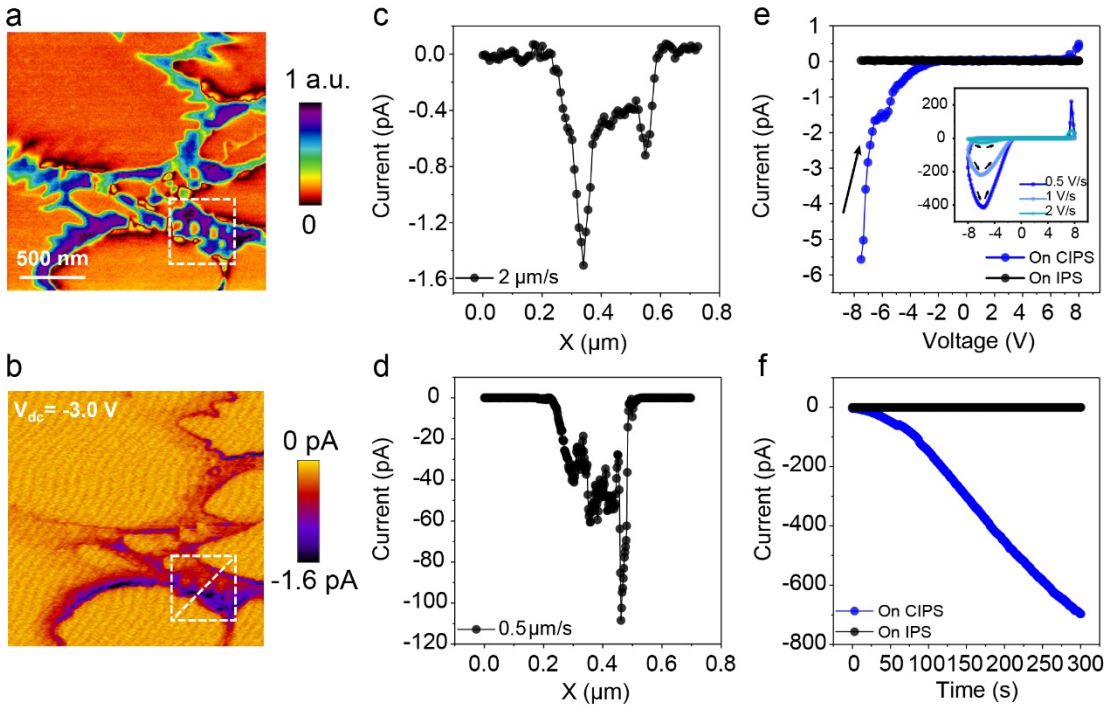

Figure 2. Electronic properties of CIPS and IPS phases at a nanoscale. **(**a) Out-of-plane PFM amplitude image. (b) c-AFM image with a tip bias of -3.0 V on the same region as (a). Current line profiles as denoted in (b) extracted from two images (of the same area indicated by the white dashed box) scanned with different speeds of 2 μm/s (c) and 0.5 μm/s (d), respectively. (e) I-V curves on the CIPS and IPS phase. The inset shows the I-V cycles with a different sweeping speed at three adjacent points. (f) The current as a function of time measured at the CIPS and IPS phases. The tip with a DC bias of -4 V was kept at fixed positions on the CIPS and IPS phases.

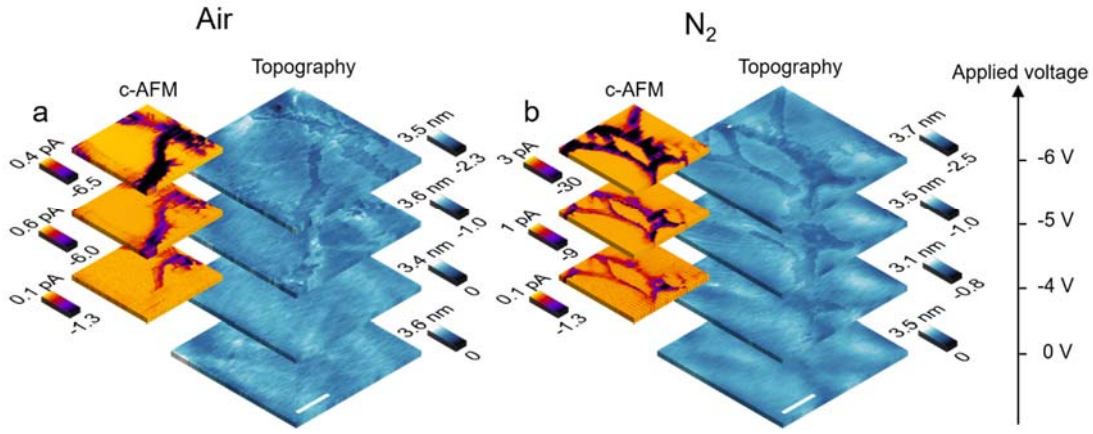

Figure 3. Electromigration of Cu in the CIPS phase. The topographical changes and c-AFM images of CIPS flakes after varied applied voltages under air (a) and N_2 (b) atmosphere are shown respectively, scale bar: 500 nm.

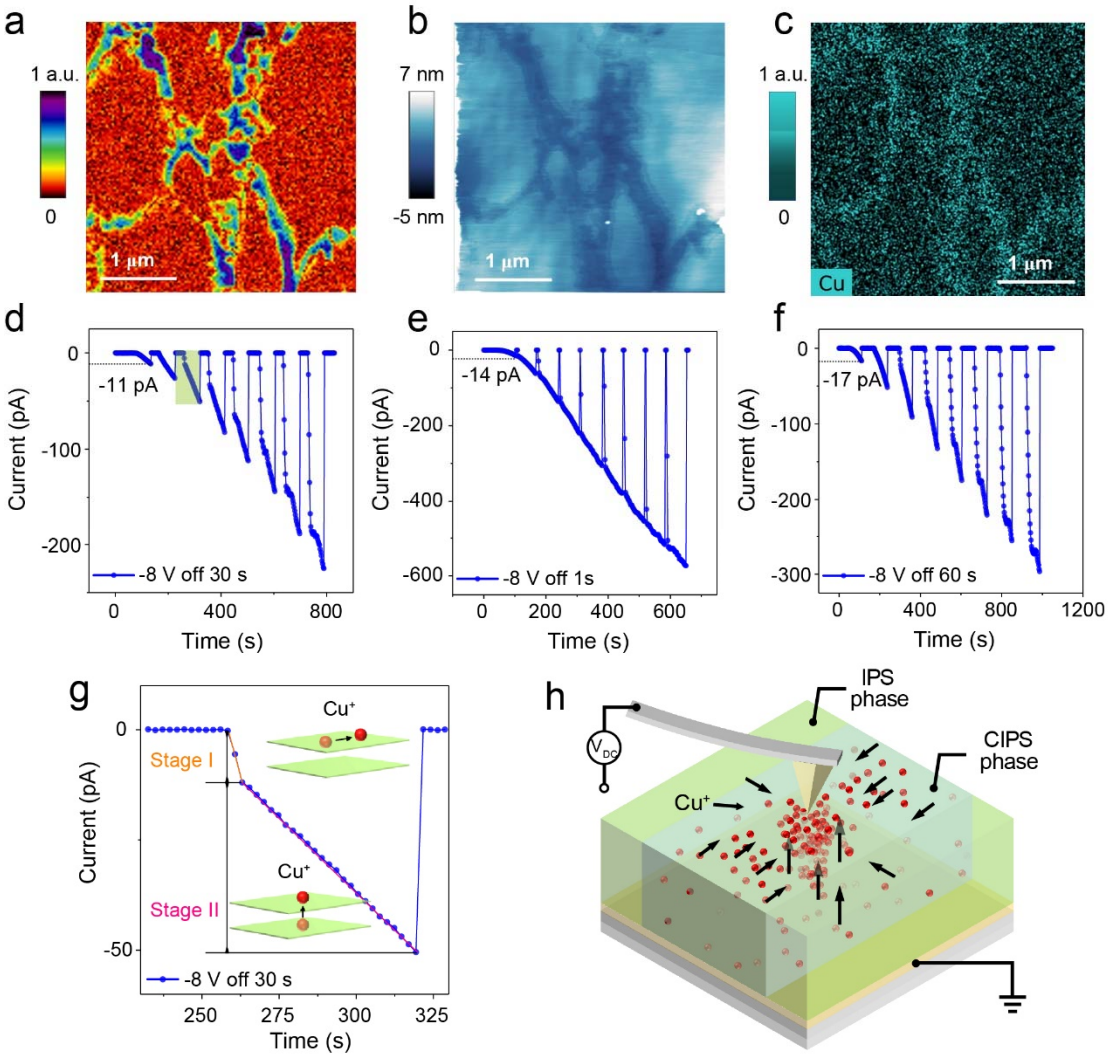

Figure 4. Nanoscale EDS evidence for Cu ion migration and directional paths revealed by time-dependent current measurements. (a) PFM amplitude of the as-grown area without the application of DC bias. The AC voltage used to acquire the image was 0.5 V. AFM topography (b) and the corresponding nanoscale SEM-EDS Cu map (c) for the same area as shown in (a) after the application of DC bias. (d-f) Detailed current measurements under a multiple of bias cycles each consisting of a same -8 V bias-on cycle of 60 s and different bias-off cycles of 30 s (d), 1 s (e), and 60 s (f). (g) A zoom-in view for the green shaded area in (d) with the time scale between 230 s to 330 s. The schematics in the inset show the Cu^+ migration paths in the OOP and IP directions. (h) Schematic illustration of Cu ion migration from both OOP and IP directions under the biased tip.

REFERENCES

(1) Zhou, S.; You, L.; Chaturvedi, A.; Morris, S. A.; Herrin, J. S.; Zhang, N.; Abdelsamie, A.; Hu, Y.; Chen, J.; Zhou, Y.; Dong, S.; Wang, J. Anomalous polarization switching and permanent retention in a ferroelectric ionic conductor. *Mater. Horiz.* **2020,** *7*, 263-274.

(2) Dziaugys, A.; Kelley, K.; Brehm, J. A.; Tao, L.; Puretzky, A.; Feng, T.; O'Hara, A.; Neumayer, S.; Chyasnavichyus, M.; Eliseev, E. A.; Banys, J.; Vysochanskii, Y.; Ye, F.; Chakoumakos, B. C.; Susner, M. A.; McGuire, M. A.; Kalinin, S. V.; Ganesh, P.; Balke, N.; Pantelides, S. T.; Morozovska, A. N.; Maksymovych, P. Piezoelectric domain walls in van der Waals antiferroelectric $CuInP_2Se_6$. *Nat. Commun.* **2020,** *11*, 3623.

(3) Deng, J.; Liu, Y.; Li, M.; Xu, S.; Lun, Y.; Lv, P.; Xia, T.; Gao, P.; Wang, X.; Hong, J. Thickness-Dependent In-Plane Polarization and Structural Phase Transition in van der Waals Ferroelectric $CuInP_2S_6$. *Small* **2020,** *16*, 1904529.

(4) Brehm, J. A.; Neumayer, S. M.; Tao, L.; O'Hara, A.; Chyasnavichus, M.; Susner, M. A.; McGuire, M. A.; Kalinin, S. V.; Jesse, S.; Ganesh, P.; Pantelides, S. T.; Maksymovych, P.; Balke, N. Tunable quadruple-well ferroelectric van der Waals crystals. *Nat. Mater.* **2020,** *19*, 43-48.

(5) Si, M.; Liao, P.-Y.; Qiu, G.; Duan, Y.; Ye, P. D. Ferroelectric field-effect transistors based on MoS_2 and $CuInP_2S_6$ two-dimensional van der Waals heterostructure. *ACS Nano* **2018,** *12*, 6700-6705.

(6) Susner, M. A.; Chyasnavichyus, M.; Puretzky, A. A.; He, Q.; Conner, B. S.; Ren, Y.; Cullen, D. A.; Ganesh, P.; Shin, D.; Demir, H.; McMurray, J. W.; Borisevich, A. Y.; Maksymovych, P.; McGuire, M. A. Cation–eutectic transition via sublattice melting in $CuInP_2S_6/In_{4/3}P_2S_6$ van der Waals layered crystals. *ACS Nano* **2017,** *11*, 7060-7073.

(7) Susner, M. A.; Chyasnavichyus, M.; McGuire, M. A.; Ganesh, P.; Maksymovych, P. Metal thio- and selenophosphates as multifunctional van der Waals layered materials. *Adv. Mater.* **2017,** *29*, 1602852.

(8) Belianinov, A.; Iberi, V.; Tselev, A.; Susner, M. A.; McGuire, M. A.; Joy, D.; Jesse, S.; Rondinone, A. J.; Kalinin, S. V.; Ovchinnikova, O. S. Polarization control via He-ion beam induced nanofabrication in layered ferroelectric semiconductors. *ACS Appl. Mater. Interfaces* **2016,** *8*, 7349-7355.

(9) Xu, D.-D.; Ma, R.-R.; Zhao, Y.-F.; Guan, Z.; Zhong, Q.-L.; Huang, R.; Xiang, P.-H.; Zhong, N.; Duan, C.-G. Unconventional out-of-plane domain inversion via in-plane ionic migration in a van der Waals ferroelectric. *J. Mater. Chem. C* **2020,** *8*, 6966-6971.

(10) Huang, W.; Wang, F.; Yin, L.; Cheng, R.; Wang, Z.; Sendeku, M. G.; Wang, J.; Li, N.; Yao, Y.; He, J. Gate-coupling-enabled robust hysteresis for nonvolatile memory and programmable rectifier in Van der Waals ferroelectric heterojunctions. *Adv. Mater.* **2020,** *32*, 1908040.

(11) Hong, X.; Posadas, A.; Zou, K.; Ahn, C. H.; Zhu, J. High-mobility few-layer graphene field effect transistors fabricated on epitaxial ferroelectric gate oxides. *Phys. Rev. Lett.* **2009,** *102*, 136808.

(12) Liu, F.; You, L.; Seyler, K. L.; Li, X.; Yu, P.; Lin, J.; Wang, X.; Zhou, J.; Wang, H.; He, H.; Pantelides, S. T.; Zhou, W.; Sharma, P.; Xu, X.; Ajayan, P. M.; Wang, J.; Liu, Z. Room-temperature ferroelectricity in $CuInP_2S_6$ ultrathin flakes. *Nat. Commun.* **2016,** *7*,

12357.
(13) Yuan, S.; Luo, X.; Chan, H. L.; Xiao, C.; Dai, Y.; Xie, M.; Hao, J. Room-temperature ferroelectricity in $MoTe_2$ down to the atomic monolayer limit. *Nat. Commun.* **2019,** *10*, 1775.
(14) Sharma, P.; Xiang, F.-X.; Shao, D.-F.; Zhang, D.; Tsymbal, E. Y.; Hamilton, A. R.; Seidel, J. A room-temperature ferroelectric semimetal. *Sci. Adv.* **2019,** *5*, eaax5080.
(15) Fei, Z.; Zhao, W.; Palomaki, T. A.; Sun, B.; Miller, M. K.; Zhao, Z.; Yan, J.; Xu, X.; Cobden, D. H. Ferroelectric switching of a two-dimensional metal. *Nature* **2018,** *560*, 336-339.
(16) Cui, C.; Hu, W.-J.; Yan, X.; Addiego, C.; Gao, W.; Wang, Y.; Wang, Z.; Li, L.; Cheng, Y.; Li, P.; Zhang, X.; Alshareef, H. N.; Wu, T.; Zhu, W.; Pan, X.; Li, L.-J. Intercorrelated in-plane and out-of-plane ferroelectricity in ultrathin two-dimensional layered semiconductor In_2Se_3. *Nano Lett.* **2018,** *18*, 1253-1258.
(17) Zheng, C.; Yu, L.; Zhu, L.; Collins, J. L.; Kim, D.; Lou, Y.; Xu, C.; Li, M.; Wei, Z.; Zhang, Y.; Edmonds, M. T.; Li, S.; Seidel, J.; Zhu, Y.; Liu, J. Z.; Tang, W.-X.; Fuhrer, M. S. Room temperature in-plane ferroelectricity in van der Waals In_2Se_3. *Sci. Adv.* **2018,** *4*, eaar7720.
(18) Zhou, Y.; Wu, D.; Zhu, Y.; Cho, Y.; He, Q.; Yang, X.; Herrera, K.; Chu, Z.; Han, Y.; Downer, M. C.; Peng, H.; Lai, K. Out-of-plane piezoelectricity and ferroelectricity in layered α-In_2Se_3 nanoflakes. *Nano Lett.* **2017,** *17*, 5508-5513.
(19) Chang, K.; Liu, J.; Lin, H.; Wang, N.; Zhao, K.; Zhang, A.; Jin, F.; Zhong, Y.; Hu, X.; Duan, W.; Zhang, Q.; Fu, L.; Xue, Q.-K.; Chen, X.; Ji, S.-H. Discovery of robust in-plane ferroelectricity in atomic-thick SnTe. *Science* **2016,** *353*, 274-278.
(20) Li, T.; Sharma, P.; Lipatov, A.; Lee, H.; Lee, J.-W.; Zhuravlev, M. Y.; Paudel, T. R.; Genenko, Y. A.; Eom, C.-B.; Tsymbal, E. Y.; Sinitskii, A.; Gruverman, A. Polarization-mediated modulation of electronic and transport properties of hybrid MoS_2–$BaTiO_3$–$SrRuO_3$ tunnel junctions. *Nano Lett.* **2017,** *17*, 922-927.
(21) Wang, X.; Yu, P.; Lei, Z.; Zhu, C.; Cao, X.; Liu, F.; You, L.; Zeng, Q.; Deng, Y.; Zhu, C.; Zhou, J.; Fu, Q.; Wang, J.; Huang, Y.; Liu, Z. Van der Waals negative capacitance transistors. *Nat. Commun.* **2019,** *10*, 3037.
(22) Zhao, M.; Gou, G.; Ding, X.; Sun, J. An ultrathin two-dimensional vertical ferroelectric tunneling junction based on $CuInP_2S_6$ monolayer. *Nanoscale* **2020,** *12*, 12522-12530.
(23) Wu, J.; Chen, H.-Y.; Yang, N.; Cao, J.; Yan, X.; Liu, F.; Sun, Q.; Ling, X.; Guo, J.; Wang, H. High tunnelling electroresistance in a ferroelectric van der Waals heterojunction via giant barrier height modulation. *Nat. Electron.* **2020,** *3*, 466-472.
(24) Macutkevic, J.; Banys, J.; Vysochanskii, Y. Electrical conductivity of layered $CuInP_2(S_xSe_{1-x})_6$ crystals. *Phys. Status Solidi B* **2015,** *252*, 1773-1777.
(25) Dziaugys, A.; Banys, J.; Macutkevic, J.; Vysochanskii, Y. Anisotropy effects in thick layered $CuInP_2S_6$ and $CuInP_2Se_6$ crystals. *Phase Transitions* **2013,** *86*, 878-885.
(26) Banys, J.; Macutkevic, J.; Samulionis, V.; Brilingas, A.; Vysochanskii, Y. Dielectric and ultrasonic investigation of phase transition in $CuInP_2S_6$ crystals. *Phase Transitions* **2004,** *77*, 345-358.
(27) Maisonneuve, V.; Reau, J. M.; Dong, M.; Cajipe, V. B.; Payen, C.; Ravez, J. Ionic conductivity in ferroic $CuInP_2S_6$ and $CuCrP_2S_6$. *Ferroelectrics* **1997,** *196*, 257-260.
(28) Yang, S. M.; Morozovska, A. N.; Kumar, R.; Eliseev, E. A.; Cao, Y.; Mazet, L.; Balke, N.;

Jesse, S.; Vasudevan, R. K.; Dubourdieu, C.; Kalinin, S. V. Mixed electrochemical–ferroelectric states in nanoscale ferroelectrics. *Nat. Phys.* **2017,** *13*, 812-818.
(29) Morozovska, A. N.; Eliseev, E. A.; Morozovsky, N. V.; Kalinin, S. V. Ferroionic states in ferroelectric thin films. *Phys. Rev. B* **2017,** *95*, 195413.
(30) Liu, Y.; Huang, Y.; Duan, X. Van der Waals integration before and beyond two-dimensional materials. *Nature* **2019,** *567*, 323-333.
(31) Liu, Y.; Weiss, N. O.; Duan, X.; Cheng, H.-C.; Huang, Y.; Duan, X. Van der Waals heterostructures and devices. *Nat. Rev. Mater* **2016,** *1*, 16042.
(32) Huang, M.; Li, S.; Zhang, Z.; Xiong, X.; Li, X.; Wu, Y. Multifunctional high-performance van der Waals heterostructures. *Nat. Nanotechnol.* **2017,** *12*, 1148-1154.
(33) Luo, Z.-D.; Xia, X.; Yang, M.-M.; Wilson, N. R.; Gruverman, A.; Alexe, M. Artificial optoelectronic synapses based on ferroelectric field-effect enabled 2D transition metal dichalcogenide memristive transistors. *ACS Nano* **2020,** *14*, 746-754.
(34) Susner, M. A.; Belianinov, A.; Borisevich, A.; He, Q.; Chyasnavichyus, M.; Demir, H.; Sholl, D. S.; Ganesh, P.; Abernathy, D. L.; McGuire, M. A.; Maksymovych, P. High-Tc layered ferrielectric crystals by coherent spinodal decomposition. *ACS Nano* **2015,** *9*, 12365-12373.
(35) Maisonneuve, V.; Cajipe, V. B.; Simon, A.; Von Der Muhll, R.; Ravez, J. Ferrielectric ordering in lamellar $CuInP_2S_6$. *Phys. Rev. B* **1997,** *56*, 10860-10868.
(36) Vysochanskii, Y. M.; Stephanovich, V. A.; Molnar, A. A.; Cajipe, V. B.; Bourdon, X. Raman spectroscopy study of the ferrielectric-paraelectric transition in layered $CuInP_2S_6$. *Phys. Rev. B* **1998,** *58*, 9119-9124.
(37) Ievlev, A. V.; Kc, S.; Vasudevan, R. K.; Kim, Y.; Lu, X.; Alexe, M.; Cooper, V. R.; Kalinin, S. V.; Ovchinnikova, O. S. Non-conventional mechanism of ferroelectric fatigue via cation migration. *Nat. Commun.* **2019,** *10*, 3064.
(38) Neumayer, S. M.; Tao, L.; O'Hara, A.; Brehm, J.; Si, M.; Liao, P.-Y.; Feng, T.; Kalinin, S. V.; Ye, P. D.; Pantelides, S. T.; Maksymovych, P.; Balke, N. Alignment of polarization against an electric field in van der Waals ferroelectrics. *Physical Review Applied* **2020,** *13*, 064063.
(39) Sharma, P.; Reece, T. J.; Ducharme, S.; Gruverman, A. High-resolution studies of domain switching behavior in nanostructured ferroelectric polymers. *Nano Lett.* **2011,** *11*, 1970-1975.
(40) Sharma, P.; Schoenherr, P.; Seidel, J. Functional Ferroic Domain Walls for Nanoelectronics. *Materials* **2019,** *12*, 2927.
(41) Sharma, P.; Sando, D.; Zhang, Q.; Cheng, X.; Prosandeev, S.; Bulanadi, R.; Prokhorenko, S.; Bellaiche, L.; Chen, L.-Q.; Nagarajan, V.; Seidel, J. Conformational Domain Wall Switch. *Adv. Funct. Mater.* **2019,** *29*, 1807523.
(42) Lindgren, G.; Canalias, C. Domain wall conductivity in $KTiOPO_4$ crystals. *APL Mater.* **2017,** *5*, 076108.
(43) Balke, N.; Neumayer, S. M.; Brehm, J. A.; Susner, M. A.; Rodriguez, B. J.; Jesse, S.; Kalinin, S. V.; Pantelides, S. T.; McGuire, M. A.; Maksymovych, P. Locally controlled Cu-ion transport in layered ferroelectric $CuInP_2S_6$. *ACS Appl. Mater. Interfaces* **2018,** *10*, 27188-27194.
(44) Chyasnavichyus, M.; Susner, M. A.; Ievlev, A. V.; Eliseev, E. A.; Kalinin, S. V.; Balke, N.; Morozovska, A. N.; McGuire, M. A.; Maksymovych, P. Size-effect in layered ferrielectric $CuInP_2S_6$. *Appl. Phys. Lett.* **2016,** *109*, 172901.

(45) Belianinov, A.; He, Q.; Dziaugys, A.; Maksymovych, P.; Eliseev, E.; Borisevich, A.; Morozovska, A.; Banys, J.; Vysochanskii, Y.; Kalinin, S. V. $CuInP_2S_6$ Room Temperature Layered Ferroelectric. *Nano Lett.* **2015,** *15*, 3808-3814.
(46) Kalinin, S. V.; Jesse, S.; Tselev, A.; Baddorf, A. P.; Balke, N. The role of electrochemical phenomena in scanning probe microscopy of ferroelectric thin films. *ACS Nano* **2011,** *5*, 5683-5691.
(47) Anantha, P. S.; Hariharan, K. ac Conductivity analysis and dielectric relaxation behaviour of $NaNO_3$–Al_2O_3 composites. *Materials Science and Engineering: B* **2005,** *121*, 12-19.
(48) Ngai, K. L. An extended coupling model description of the evolution of dynamics with time in supercooled liquids and ionic conductors. *J. Phys.: Condens. Matter* **2003,** *15*, S1107-S1125.